4′-[Methyl-^{11}C]-Thiothymidine PET/CT for Proliferation Imaging in Non–Small Cell Lung Cancer

Ryogo Minamimoto[1], Jun Toyohara[2], Ayako Seike[3], Hideyuki Ito[3], Hisako Endo[4], Miyako Morooka[1], Kazuhiko Nakajima[1], Takuya Mitsumoto[1], Kimiteru Ito[1], Momoko Okasaki[1], Kiichi Ishiwata[2], and Kazuo Kubota[1]

[1]Division of Nuclear Medicine, Department of Radiology, National Center for Global Health and Medicine, Tokyo, Japan; [2]Positron Medical Center, Tokyo Metropolitan Institute of Gerontology, Tokyo, Japan; [3]Department of Thoracic Surgery, National Center for Global Health and Medicine, Tokyo, Japan; and [4]Division of Pathology, Department of Central Laboratory, National Center for Global Health and Medicine, Tokyo, Japan

A new tracer, 4′-[methyl-^{11}C]-thiothymidine (^{11}C-4DST), has been developed as an in vivo cell proliferation marker based on the DNA incorporation method. This study evaluated the potential of ^{11}C-4DST PET/CT for imaging proliferation in non–small cell lung cancer (NSCLC), compared with ^{18}F-FDG PET/CT. **Methods:** Eighteen patients with lung lesions were examined by PET/CT using ^{11}C-4DST and ^{18}F-FDG. We constructed decay-corrected time–activity curves of 9 major regions as the mean standardized uptake value. We then compared the maximum standardized uptake value (SUVmax) of lung tumors on both ^{11}C-4DST and ^{18}F-FDG PET/CT with the Ki-67 index of cellular proliferation and with CD31-positive vessels as a marker of angiogenesis in surgical pathology. **Results:** NSCLC was pathologically confirmed in 19 lesions of 18 patients. Physiologic accumulation of ^{11}C-4DST was high in liver, kidney, and bone marrow and low in aorta, brain, lung, and myocardium. Biodistribution of ^{11}C-4DST was almost stable by 20 min after injection of ^{11}C-4DST. Mean ^{11}C-4DST SUVmax for lung cancer was 2.9 ± 1.0 (range, 1.5–4.7), significantly different from mean ^{18}F-FDG SUVmax, which was 6.2 ± 4.5 (range, 0.9–17.3; $P < 0.001$). The correlation coefficient between SUVmax and Ki-67 index was higher with ^{11}C-4DST ($r = 0.82$) than with ^{18}F-FDG ($r = 0.71$). The correlation coefficient between SUVmax and CD31 was low with both ^{11}C-4DST ($r = 0.21$) and ^{18}F-FDG ($r = 0.21$), showing no significant difference between the tracers. **Conclusion:** A higher correlation with proliferation of lung tumors was seen for ^{11}C-4DST than for ^{18}F-FDG. ^{11}C-4DST PET/CT may allow noninvasive imaging of DNA synthesis in NSCLC.

Key Words: 4DST; FDG; PET/CT; non–small cell lung cancer; cell proliferation

J Nucl Med 2012; 53:199–206
DOI: 10.2967/jnumed.111.095539

Uncontrolled proliferation is a distinctive characteristic of cancer cells (*1*). The ability to image cellular proliferation would offer the possibility of distinguishing between benign and malignant tissues, measuring tumor activity, and evaluating response to therapy (*2*). Cellular proliferation is thus a key characteristic in oncology, and its imaging has been a critical goal of nuclear medicine.

Proliferating cells synthesize DNA during the S phase of the cell cycle. The pyrimidine analog thymidine is incorporated into DNA but not into RNA. DNA incorporation of ^{3}H-thymidine is considered the gold standard for characterizing cell proliferation (*1,2*).

The first PET tracer for imaging cellular proliferation was thymidine labeled with ^{11}C at the methyl group (methyl-^{11}C-thymidine) (*3*). However, degradation in vivo resulted in ambiguous evidence for imaging of cellular proliferation. Assessment of thymidine flux from blood into DNA has been clarified in a multicompartment, metabolite-corrected kinetic model of imaging data using thymidine labeled with ^{11}C at the 2-position (2-^{11}C-thymidine) in somatic and brain tumors (*4–7*). However, the complexity of 2-^{11}C-thymidine PET in terms of methods and analysis seems likely to preclude widespread clinical use in cellular proliferation imaging. Although 3′-deoxy-3′-^{18}F-fluorothymidine (^{18}F-FLT) has achieved good clinical results for cellular proliferation imaging (*8*), ^{18}F-FLT is not incorporated into DNA because of the lack of a 3′-hydroxyl, unlike thymidine. As a result, ^{18}F-FLT imaging is regarded as the salvage pathway of DNA synthesis (*2*).

Toyohara et al. developed 4′-thiothymidine labeled with ^{11}C at the methyl group (4′-[methyl-^{11}C]-thiothymidine [^{11}C-4DST], previously designated as ^{11}C-S-dThd) as a new candidate tracer for cell proliferation imaging that is resistant to degradation by thymidine phosphorylase and is incorporated into DNA (*9,10*). Moreover, ^{14}C-4DST has shown significantly higher uptake into proliferating tissues than FLT labeled with ^{3}H at the methyl group, a result supported by an animal study using ^{11}C-4DST (*10*). In a human study using ^{11}C-4DST, Toyohara et al. showed that true input curves after metabolite analysis and dynamic brain tumor imaging resulted in a linear Patlak plot over

Received Jul. 11, 2011; revision accepted Oct. 4, 2011.
For correspondence or reprints contact: Ryogo Minamimoto, Division of Nuclear Medicine, Department of Radiology, National Center for Global Health and Medicine, 1-21-1, Toyama, Shinjyuku-ku, Tokyo, 162-8655, Japan.
E-mail: ryogominamimoto@yahoo.co.jp
Published online Dec. 21, 2011.

10–90 min after injection and suggested metabolic incorporation of 4DST into higher molecules, such as DNA (*11*).

An ^{11}C-4DST PET study of patients with brain tumor showed that ^{11}C-4DST PET is feasible for brain tumor imaging and can be performed with acceptable dosimetry and pharmacologic safety at a suitable dose for adequate imaging (*11*). Individual-organ and total-body doses associated with ^{11}C-4DST are reportedly lower than those with ^{18}F-FLT (*11,12*). Although the short physical half-life of ^{11}C places a significant limitation on counting statistics and commercial convenience for widespread routine clinical use, diagnosis using multiple tracers to determine tumor characteristics is possible, and repeated scans during the course of therapy are feasible given the lower radiation burden.

These results indicate that ^{11}C-4DST has great potential for imaging cell proliferation, but this potential needs to be confirmed in a variety of cancers. Tumor cell proliferation is one of the most significant predictors of prognosis for patients with cancers such as non–small cell lung cancer (NCSLC) (*13*). The present study evaluated the potential of ^{11}C-4DST PET/CT, compared with ^{18}F-FDG PET/CT, for imaging proliferation in NSCLC.

MATERIALS AND METHODS

Patients

This prospective study was approved by the institutional review board at our facility, and written informed consent was obtained from all patients before participation. A total of 18 patients (12 men and 6 women; mean (±SD) age, 68.1 ± 9.4 y; range, 55–84 y) with histologically confirmed NSCLC were included in this study. All patients underwent chest CT before ^{11}C-4DST and ^{18}F-FDG PET/CT examinations, which were performed before surgical resection of the lung lesion.

^{11}C-4DST PET/CT Examination

The ^{11}C-4DST was synthesized as previously described (*11*). PET/CT images were obtained using a system (Biograph 16; Siemens) consisting of a PET scanner and multidetector-row CT scanner (16 detectors), measuring from vertex to thigh. All subjects fasted for 5 h before receiving an intravenous injection of ^{11}C-4DST within the range of 666–777 MBq. Low-dose CT was performed first and was used for attenuation correction and image fusion. Emission images were acquired in 3-dimensional mode for 2 min/bed position to obtain an image at 5 min after intravenous injection of ^{11}C-4DST and 2.5 min/bed position to obtain images at 20, 40, 60, and 80 min after intravenous injection of ^{11}C-4DST. PET data were reconstructed using a gaussian filter with an ordered-subset expectation maximization algorithm (3 iterations, 8 subsets). Images with ^{11}C-4DST were obtained from all patients at 40 min after intravenous injection of ^{11}C-4DST. Additional ^{11}C-4DST images were obtained from some patients at 5 min ($n = 5$), 20 min ($n = 6$), 60 min ($n = 9$), and 80 min ($n = 9$) after intravenous injection of ^{11}C-4DST.

^{18}F-FDG PET/CT Examination

An in-house cyclotron and automated synthesis system (F100; Sumitomo Heavy Industries) was used in accordance with the authorized procedure to synthesize ^{18}F-FDG. All subjects fasted for 5 h before blood glucose levels were measured and ^{18}F-FDG intravenously injected (370 MBq). PET/CT images were obtained at 60 min after injection with the same method as for ^{11}C-4DST. For 13 patients, ^{18}F-FDG PET/CT scans were obtained 90 min or more after the ^{11}C-4DST PET/CT scans. For the other patients, the interval between ^{11}C-4DST and ^{18}F-FDG PET/CT was 2 d for 1 patient, 5 d for 1 patient, 11 d for 1 patient, and 23 d for 2 patients.

PET Data Analysis

All ^{11}C-4DST and ^{18}F-FDG PET/CT scans were evaluated by 2 experienced nuclear medicine physicians who were unaware of the clinical data. Regions of interest were placed in the lung lesion according to CT images obtained from PET/CT, and maximum standardized uptake value (SUVmax) and mean standardized uptake value (SUVmean) were determined for ^{11}C-4DST and ^{18}F-FDG PET/CT images, respectively. Regions of interest were placed in the following organs: ascending aorta (blood pool), brain, lungs, myocardium, liver, kidneys, muscle, and bone marrow. The decay-corrected time–activity curves of 9 regions (8 organs and the tumor) were identified as the mean of SUVmeans recorded from 18 patients according to imaging time.

Ki-67 and CD31 Staining

Staining was performed using the ChemMate EnVision method (Dako) with an auto-staining system (Dako Autostainer) in accordance with the protocol provided by the manufacturer. Formalin-fixed and paraffin-embedded sections (3 μm) of resected specimens from lung cancer were taken for immunohistochemical staining. Antigen was retrieved by heating after immersion of tissue slides into citrate buffer (pH 6.0) in an autoclave at 121°C for 10 min. Mouse monoclonal antibodies specific for Ki-67 (MIB-1; Dako) and CD31 (JC70A; Dako) were used at dilutions of 1:25 and 1:40, respectively. This study also used 3,3′-diaminobenzidine as the final chromogen and hematoxylin as the nuclear counterstain.

Ki-67 index was estimated by counting the percentage of Ki-67–positive cell nuclei per 2,500–10,000 tumor cells in 5 regions with ×200 magnification of the tumor part showing the greatest staining density, in most instances corresponding to the areas of highest mitotic activity.

Microvessel density was assessed using the criteria of Weidner et al. (*14*). Areas of highest neovascularization were identified as regions of invasive carcinoma with the highest numbers of discrete microvessels stained for CD31. Vessel number was assessed by counting CD31-positive vessels (with a clearly defined lumen or well-defined linear vessel shape but not single endothelial cells) in 5 representative regions with ×200 magnification. Histopathologic slides were examined by a pathologist who was unaware of clinical data and PET findings.

Statistical Analysis

The significance of differences between SUVmax and SUVmean for ^{11}C-4DST and ^{18}F-FDG in the primary lesion was determined using paired t tests. Correlations between ^{11}C-4DST and ^{18}F-FDG uptake and Ki-67 labeling index or number of CD31-stained vessels were assessed using linear regression analysis. Statistical significance was considered to be present for values of P less than 0.05.

RESULTS

Pathologic Findings

Pathologic analysis revealed adenocarcinoma in 15 patients (16 lesions), squamous cell carcinoma in 2 patients, and large cell carcinoma in 1 patient. In 2 patients,

the adenocarcinoma was bronchioloalveolar carcinoma. The mean diameter of the lung lesion was 27.2 ± 14.4 mm (range, 12.0–62.0 mm). Lymph node metastases were histopathologically diagnosed in 5 patients (Table 1).

Whole-Body Imaging

Maximum-intensity-projection images and axial images of ^{11}C-4DST PET are shown in Figures 1 and 2, respectively. High physiologic ^{11}C-4DST uptake was observed in the salivary glands, liver, spleen, kidneys, bladder, and bone marrow. In contrast, the brain, lungs, myocardium, muscle, and blood pool showed low physiologic ^{11}C-4DST uptake.

Figure 3 illustrates the decay-corrected time–activity curves of ^{11}C-4DST in patients with lung cancer. Radioactivity in the blood pool was low by 5 min after injection, and levels in myocardium, lung, and muscle decreased slightly over time. Radioactivity was excreted from the kidneys and was considered to peak less than 5 min after ^{11}C-4DST injection. In the liver and bone marrow, radioactivity remained high from 5 min onward after ^{11}C-4DST injection. Uptake of ^{11}C-4DST in the tumor was relatively high from 5 min onward after ^{11}C-4DST injection and increased slightly over time.

Comparison of ^{11}C-4DST and ^{18}F-FDG Uptake in Lung Lesions

All malignant lesions showed focal increases in uptake of ^{11}C-4DST and ^{18}F-FDG (Table 1). The mean SUVmax and SUVmean of ^{11}C-4DST for lung lesions were 2.9 ± 1.0 (range, 1.5–4.7) and 1.7 ± 0.4 (range, 1.0–2.5), respectively. The mean SUVmax and SUVmean of ^{18}F-FDG for lung lesions were 6.2 ± 4.5 (range, 0.9–17.3) and 2.6 ± 1.4 (range, 0.6–5.8), respectively. Uptake by lung tumors was significantly higher for ^{18}F-FDG than for ^{11}C-4DST ($P < 0.001$). Linear regression analysis of ^{11}C-4DST and ^{18}F-FDG yielded a correlation coefficient of 0.73 ($P < 0.001$) for SUVmax (Fig. 4) and 0.79 ($P < 0.001$) for SUVmean.

Ki-67 and CD31 Immunohistochemistry

Ki-67 immunohistochemical staining was assessed in all 19 lesion specimens obtained by surgical resection. The mean interval between ^{11}C-4DST PET/CT and surgery was 15 ± 27 d (range, 1–110 d). All NSCLC specimens contained Ki-67–positive cells. The mean proliferation fraction was 50.9% ± 29.1% (range, 4%–92%) (Table 1). Linear regression analysis identified a significant correlation between the SUVmax of ^{11}C-4DST and Ki-67 index ($r = 0.82$; $P < 0.001$; Fig. 5A). A significant correlation was also observed between the SUVmax of ^{18}F-FDG uptake and Ki-67 index ($r = 0.71$; $P < 0.001$; Fig. 5B), but this correlation was lower than that for ^{11}C-4DST.

CD31 immunohistochemical staining was assessed in all 19 lesion specimens obtained by surgical resection. All NSCLC specimens contained CD31-positive vessels (Table 1). Linear regression analysis indicated no significant cor-

TABLE 1
Patient Characteristics

Patient no.	Age (y)	Sex	Histology	TNM stage	Tumor diameter (mm)	Standardized uptake value				Ki-67 index (%)	CD31-positive vessels (*n*)
						^{11}C-4DST	^{18}F-FDG				
						Maximum	Mean	Maximum	Mean		
1	56	M	Adenocarcinoma	pT2N0M0	31	4.7	2.2	10.9	3.7	81	816
2	79	F	Adenocarcinoma	pT1N0M0	14	1.8	1.1	1.3	0.7	16	381
			Adenocarcinoma		18	2.1	1.2	2.8	1.6	29	410
3	55	F	Adenocarcinoma	pT1N0M0	18	4.1	1.5	7.7	2.4	92	769
4	60	M	Adenocarcinoma	pT1N1M0	15	1.5	1.1	1.4	1.1	18	485
5	69	M	Adenocarcinoma	pT3N1M0	12	2.7	1.8	13.7	5.7	67	579
6	62	M	Adenocarcinoma	pT2N0M0	32	3.5	2.1	7.1	2.7	20	464
7	77	F	Adenocarcinoma	pT1N0M0	20	2.7	1.7	4.5	1.8	72	423
8	73	F	Adenocarcinoma	pT2N0M0	15	2.7	1.7	5.2	2.5	35	362
9	58	M	Squamous cell carcinoma	pT2N1M0	30	3.0	2.0	5.6	2.8	62	309
10	55	M	Large cell carcinoma	pT2N1M0	62	3.2	1.8	7.6	3.2	74	717
11	72	M	Adenocarcinoma	pT2N0M0	55	4.5	2.5	10.1	4.9	79	1,042
12	74	M	Squamous cell carcinoma	pT2N0M0	30	3.9	2.3	17.3	4.7	87	1,565
13	78	M	Adenocarcinoma	pT2N0M0	38	4.0	2.1	6.3	3.1	76	366
14	73	M	Adenocarcinoma*	pT1N0M0	20	2.1	1.3	3.6	2.4	19	622
15	79	M	Adenocarcinoma	pT1N0M0	19	3.0	1.7	4.2	2.5	76	3,102
16	58	F	Adenocarcinoma	pT1N2M0	18	1.5	1.5	3.5	2.3	45	884
17	63	F	Adenocarcinoma	pT2N0M0	32	1.6	1.3	0.8	0.6	4	780
18	84	M	Adenocarcinoma*	pT1N0M0	19	1.9	1.4	1.2	0.7	18	485

*Bronchioloalveolar carcinoma.

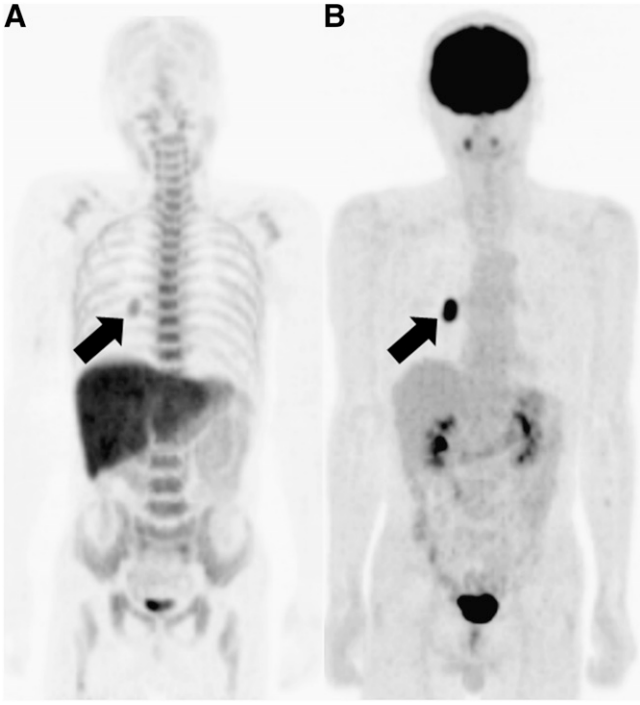

FIGURE 1. Maximum-intensity-projection images of ^{11}C-4DST PET (A) and ^{18}F-FDG PET (B) in patient 1 with lung adenocarcinoma. Compared with physiologic ^{18}F-FDG uptake, physiologic ^{11}C-4DST uptake is high in salivary glands, liver, and bone marrow and low in brain, kidney, and muscle. Focal uptake in lung tumor in right lower lobe is confirmed on ^{11}C-4DST PET and ^{18}F-FDG PET images (arrow). ^{11}C-4DST uptake in tumor lesion is lower than ^{18}F-FDG uptake.

relation between SUVmax for ^{11}C-4DST and microvessel density as determined by CD31 staining ($r = 0.21$; $P < 0.001$). Likewise, no significant correlation was observed between CD31-microvessel density and SUVmax for ^{18}F-FDG ($r = 0.21$; $P < 0.001$), which was equal to that for ^{11}C-4DST.

DISCUSSION

In the present study, ^{11}C-4DST ($r = 0.82$) showed a higher correlation with cell proliferation as evaluated by Ki-67 index in NSCLC than did ^{18}F-FDG ($r = 0.71$), confirming ^{11}C-4DST PET/CT as a useful noninvasive modality for imaging DNA synthesis by NSCLC.

Proliferation rate is a known prognostic marker for the survival of patients with NSCLC (*15*). PET proliferation imaging should thus have an impact on oncology as a noninvasive clinical approach, and the present study demonstrated the high potential of ^{11}C-4DST. The structure of ^{11}C-4DST has the 4′-oxo of thymidine replaced by 4′-sulfur, so as to closely resemble the structure of thymidine (*16*). An in vitro study proved that ^{3}H-4DST is incorporated into DNA (*17*), and ^{14}C-4DST was confirmed to show metabolism similar to that of thymidine, maintaining stability in the blood (*9,10*). In a human study, Toyohara et al. used Patlak graphical analysis to obtain the ^{11}C-4DST flux constant (K_i), and K_i values of ^{11}C-4DST correlated well with standardized uptake value (*11*). These data support the idea that 4DST would be incorporated into DNA in the human body. However, DNA incorporation of 4DST does not entirely mean that 4DST can quantify the DNA synthesis ratio. 4DST uptake reflects multiple steps: sustained delivery and transport of the tracer, metabolic trapping as a phosphorylated form, or DNA synthesis. The rate-limiting step for tissue retention of 4DST should thus be determined to clarify the trapping mechanisms of 4DST.

In a human study, ^{11}C-4DST was metabolized to hydrophilic metabolites, and at least 5 radioactive metabolites were detected. In urine, 2 hydrophilic metabolites were dominant, and one of these was also commonly detected in plasma (*11*).

Serum thymidine may compete with nucleoside tracers for the active site of nucleoside carriers in cell membranes and for the active site of the trapping enzyme, thymidine

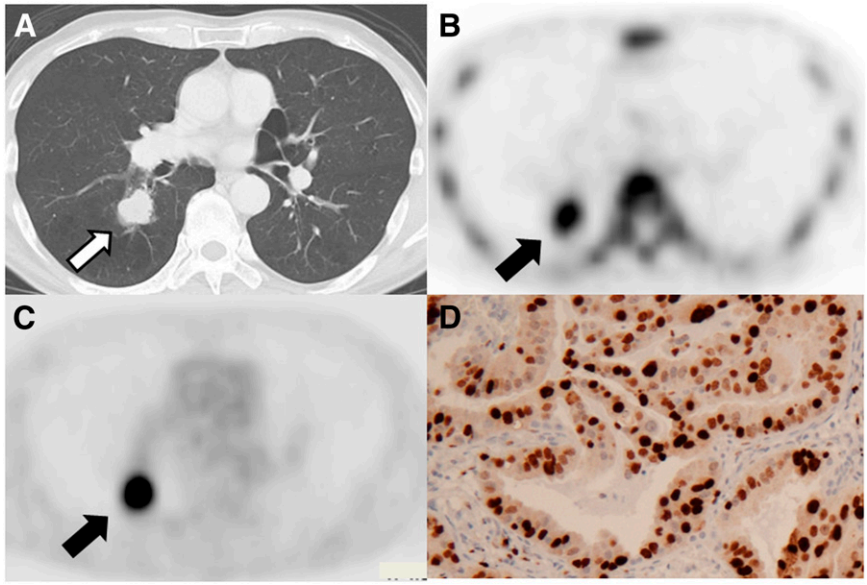

FIGURE 2. Axial images of CT (A), ^{11}C-4DST PET (B), and ^{18}F-FDG PET (C) in patient 1 with lung adenocarcinoma in right lower lobe (arrow). Radioactivity of ^{11}C-4DST in ascending aorta (representing blood pool) was lower than that of ^{18}F-FDG. Both ^{11}C-4DST and ^{18}F-FDG clearly accumulate in lung lesions, and ^{11}C-4DST uptake (SUVmax, 4.7) is lower than ^{18}F-FDG uptake (SUVmax, 10.9). On Ki-67 immunohistochemistry (D), Ki-67–positive nuclei (colored brown) show estimated proliferation rate of 81%.

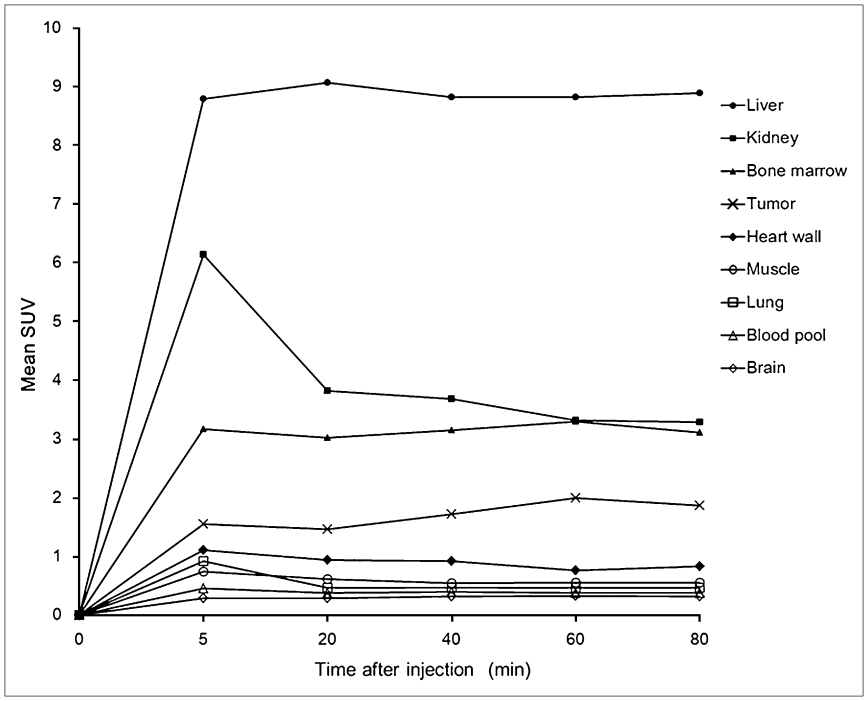

FIGURE 3. Decay-corrected time–activity curves of ^{11}C-4DST for major organs, measured as SUVmean.

kinase 1. Currently, we have no detailed information on the affinities or subtype selectivities of 4DST toward nucleoside transporters and thymidine kinase. Despite a high serum thymidine concentration, previous rodent studies of ^{11}C-4DST have been performed with no phosphorylase pretreatment (*9,10*). Therefore, in contrast to ^{18}F-FLT, competition of endogenous thymidine for ^{11}C-4DST uptake appears negligible.

Although the detailed mechanisms underlying ^{11}C-4DST uptake are not well understood in humans, the biodistribution of ^{11}C-4DST was nearly identical to that of ^{18}F-FLT, which is linked to the S-phase–specific enzyme thymidine kinase, suggesting that ^{11}C-4DST PET may reflect cell proliferation via this kinase (*18,19*). In addition, low ^{11}C-4DST uptake in myocardium indicated a low affinity for TK2, a mitochondrial isozyme unrelated to cellular proliferation.

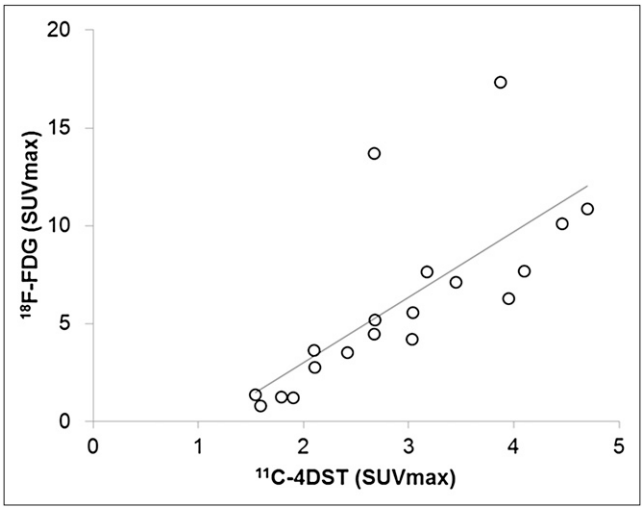

FIGURE 4. Linear regression analysis showing significant correlation of SUVmax ($r = 0.73$, $P < 0.001$) between ^{11}C-4DST uptake and ^{18}F-FDG uptake in lung lesion.

Uptake of ^{11}C-4DST by NSCLC was about 50% lower than that of ^{18}F-FDG, as seems similar to the relationship between ^{18}F-FLT and ^{18}F-FDG. We were able to measure ^{11}C-4DST uptake for tumor lesions because we placed regions of interest on solitary lung lesions based on CT results; therefore, negative findings for the lesion were not obtained for our study cases. Given the small number of cases showing lymph node metastasis in this study, evaluating the potential of ^{11}C-4DST for diagnosing lymph node metastasis is difficult. A relatively low accumulation of ^{11}C-4DST could lead to failure to detect some lesions, representing a crucial problem as seen for ^{18}F-FLT. As a result, ^{11}C-4DST PET may be best positioned for prediction of patient prognosis rather than detection or staging of cancers. We performed ^{18}F-FDG examinations after the completion of ^{11}C-4DST examinations for most of the patients included in this study. This protocol could provide information within half a day regarding staging of lung cancer by ^{18}F-FDG and proliferation in the primary lesion by 4DST labeled with ^{11}C, which shows a relatively short half-life.

The correlation coefficient for ^{18}F-FDG uptake and proliferative activity (Ki-67) in pulmonary nodules has been reported to be in the range of 0.59–0.73 (*20–22*). Our result ($r = 0.71$) supports this finding. Yamamoto et al. revealed a high correlation coefficient ($r = 0.81$) between ^{18}F-FDG uptake and proliferative activity, compared with an estimated 0.63 among patients with adenocarcinoma, which

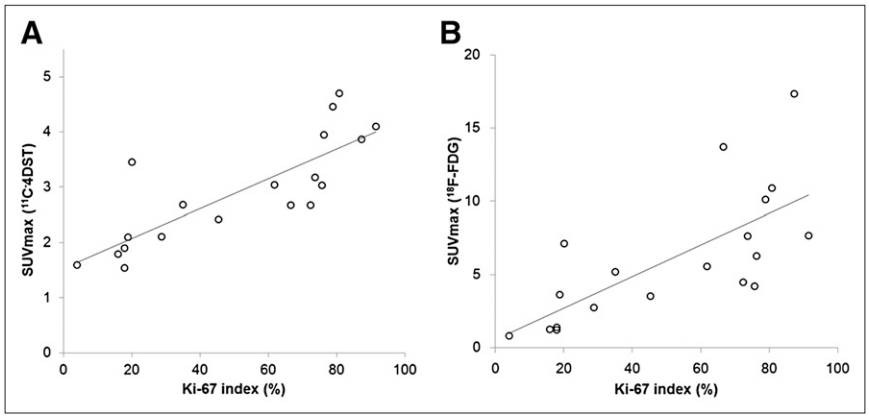

FIGURE 5. Linear regression analysis showing significant correlation between SUVmax of ^{11}C-4DST and proliferative activity (Ki-67 index) (A) ($r = 0.82$; $P < 0.001$). Significant correlation is also observed between SUVmax for ^{18}F-FDG uptake and Ki-67 index (B) ($r = 0.71$; $P < 0.001$).

was the most common tumor in our study (*23*). The correlation coefficient for ^{18}F-FLT uptake and proliferative activity in pulmonary nodules was within the range of 0.77–0.87 (*8*). However, this coefficient was calculated from lesions that included inflammatory lesions. The correlation coefficient for ^{18}F-FLT uptake (SUVmax) and proliferative activity in any NSCLC was estimated to be within the range of 0.59–0.83. Our study showed ^{11}C-4DST to have a higher correlation coefficient ($r = 0.82$) than ^{18}F-FDG ($r = 0.71$) for uptake and proliferative activity in NSCLC. However, further study with larger numbers of patients is needed to evaluate the reliability of ^{11}C-4DST as a proliferation imaging tracer.

Regarding angiogenesis, no significant correlation between ^{18}F-FDG uptake and CD31-microvessel density has been reported (*24*), again supported by the present results. The correlation coefficient between ^{11}C-4DST uptake and CD31-microvessel density was low, with no difference from that between ^{18}F-FDG uptake and CD31-microvessel density. According to the regional time–activity curve, ^{11}C-4DST uptake for lung lesions increased slightly over time, even though radioactivity in the ascending aorta (representing the blood pool) remained low over the course of 80 min from injection. These results might indicate that ^{11}C-4DST uptake for tumor lesions did not depend on blood flow, with steady uptake by the tumor and incorporation into DNA in relation to cell proliferation. Toyohara et al. used Patlak graphical analysis to obtain the ^{11}C-4DST K_i, and K_i values of ^{11}C-4DST correlated well with standardized uptake value (*11*). Our study showed a higher correlation coefficient between ^{11}C-4DST uptake and Ki-67% index. As a result, ^{11}C-4DST was expected to work as a marker of DNA synthesis.

One limitation of this study was that we could not obtain dynamic ^{11}C-4DST scan data, because of the nonintegrated dynamic scan mode in the PET/CT scanner. We failed to obtain a specific regional time–activity curve and ^{11}C-4DST flux estimate from Patlak plot analysis; however, the ^{11}C-4DST biodistribution tendency was same as the study data in patients with brain tumor described by Toyohara et al. (*11*). Another limitation was the relatively long period between ^{11}C-4DST scanning and surgery, compared with other

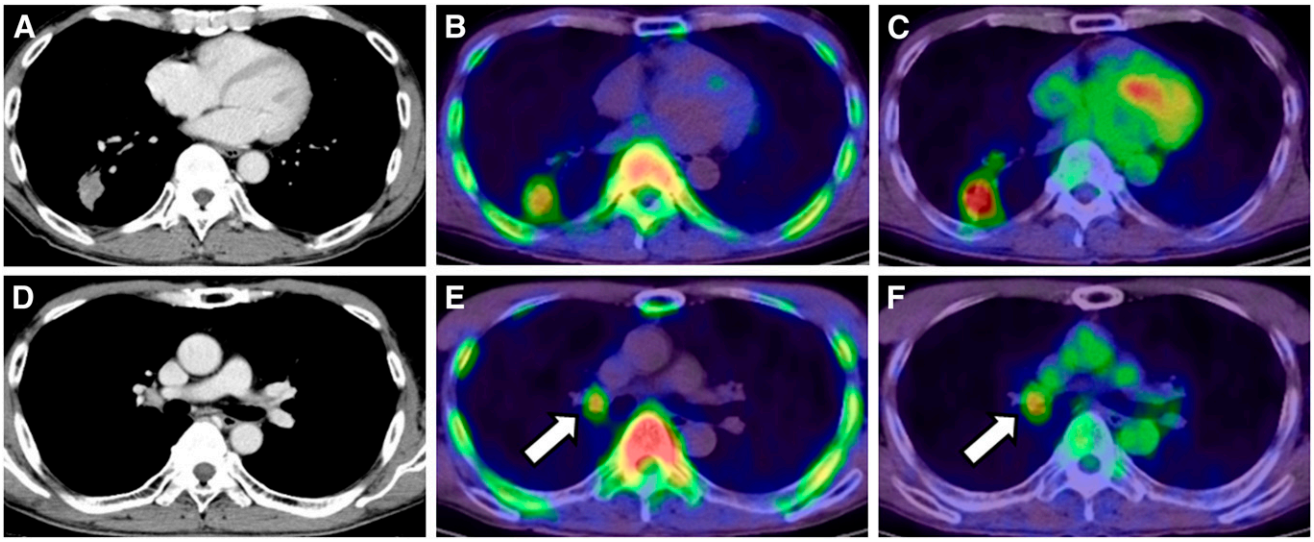

FIGURE 6. Axial images of CT (A), ^{11}C-4DST PET (B), and ^{18}F-FDG PET (C) in patient 9 with lung adenocarcinoma in right lower lobe. Right hilar lymph node metastasis is confirmed on CT (D), and uptake on both ^{11}C-4DST PET (E) and ^{18}F-FDG PET (F) identifies lesion (arrow). However, ^{11}C-4DST image is clearer than ^{18}F-FDG image because of low physiologic ^{11}C-4DST in mediastinum as blood pool.

studies, and 2 patients showed exceptionally long intervals of 37 and 110 d, attributed to events largely unrelated to this study. However, SUVmax and SUVmean in these 2 patients were plotted near the correlation line obtained from linear regression analysis.

We set a duration of more than 90 min between ^{11}C-4DST and ^{18}F-FDG studies, when the 2 scans were obtained on the same day (13 patients). The effect of remnant radioactivity from the ^{11}C-4DST scan on ^{18}F-FDG uptake in patients undergoing 2 sessions of PET within a single day can be considered negligible. For a study with ^{11}C-methionine and ^{18}F-FDG, a 90-min interval has been considered to avoid contamination by sites of high ^{11}C-methionine accumulation, such as the liver (unpublished data). Because high-accumulation sites tended to be similar for ^{11}C-4DST and ^{11}C-methionine, we applied the same interval to the studies with ^{11}C-4DST and ^{18}F-FDG.

We set a common scan time of 40 min after ^{11}C-4DST injection. According to the regional time–activity curve, the radioactivity level in tumors increased slightly over time, whereas that in the blood pool was stable from 5 min after injection. The scanning time at 20 min after ^{11}C-4DST was the same as that at 40 and 60 min, but a relatively high deviation in ^{11}C-4DST biodistribution was confirmed in our study and in a study on a patient with a brain tumor (*11*). Tumor-to-blood ratio was thus highest at 60 min after ^{11}C-4DST injection, representing the best time for tumor imaging. However, scan images obtained within 40 min after injection yielded almost the same tumor-to-blood ratio. To reduce the injected radiation dose, 40 min rather than 60 min appears to represent the best scan time for evaluation of lung tumor.

Respiratory artifacts can be observed on CT images and induce errors in attenuation-corrected PET images (*25*), including standardized uptake value (*26*). To minimize this effect, PET and CT acquisitions were performed during shallow breathing (*27*). All lung nodules in this study were over 1 cm in diameter and not close to the diaphragm. Our study results could avoid artifacts.

^{11}C-4DST also accumulated at lymph node metastases (Fig. 6.), but evaluation of lymph nodes requires further investigation because of the small number of patients with lymph node metastases ($n = 5$).

The potential of ^{11}C-4DST PET for distinguishing between inflammation and malignancy could not be evaluated in this study.

The most crucial application for cell proliferation is monitoring antiproliferative therapy, and Toyohara et al. showed a case in which ^{11}C-4DST PET had potential for monitoring cancer treatment response (*11*). Further clinical studies are needed to address these issues.

CONCLUSION

Proliferation of lung tumors correlated better with ^{11}C-4DST uptake than with ^{18}F-FDG uptake, supporting ^{11}C-4DST PET/CT as a noninvasive modality for imaging DNA synthesis in NSCLC.

DISCLOSURE STATEMENT

The costs of publication of this article were defrayed in part by the payment of page charges. Therefore, and solely to indicate this fact, this article is hereby marked "advertisement" in accordance with 18 USC section 1734.

ACKNOWLEDGMENTS

We thank Takashi Sato, Toshiaki Fujita, Shingo Kawaguchi, and Yoshiaki Taguchi for technical support. This work was supported by grant 21 A-26 from the National Center for Global Health and Medicine and grant-in-aid 22390241 for scientific research (B) from the Japan Society for the Promotion of Science. No other potential conflict of interest relevant to this article was reported.

REFERENCES

1. Bading JR, Shields AF. Imaging of cell proliferation: status and prospects. *J Nucl Med.* 2008;49(suppl):64S–80S.
2. Been LB, Suurmeijer AJ, Cobben DC, Jager PL, Hoekstra HJ, Elsinga PH. [^{18}F] FLT-PET in oncology: current status and opportunities. *Eur J Nucl Med Mol Imaging.* 2004;31:1659–1672.
3. Christman D, Crawford EJ, Friedkin M, Wolf AP. Detection of DNA synthesis in intact organisms with positron-emitting [methyl-^{11}C]thymidine. *Proc Natl Acad Sci USA.* 1972;69:988–992.
4. Schields AF, Mankoff DA, Link JM, et al. Carbon-11-thymidine and FDG to measure therapy response. *J Nucl Med.* 1998;39:1757–1762.
5. Mankoff DA, Shields AF, Link JM, et al. Kinetic analysis of 2-[^{11}C]thymidine PET imaging studies: validation studies. *J Nucl Med.* 1999;40:614–624.
6. Wells JM, Mankoff DA, Eary JF, et al. Kinetic analysis of 2-[^{11}C]thymidine PET imaging studies of malignant brain tumors: preliminary patient results. *Mol Imaging.* 2002;1:145–150.
7. Wells JM, Mankoff DA, Muzi M, et al. Kinetic analysis of 2-[^{11}C]thymidine PET imaging studies of malignant brain tumors: compartmental model investigation and mathematical analysis. *Mol Imaging.* 2002;1:151–159.
8. Shields AF, Grierson JR, Dohmen BM, et al. Imaging proliferation *in vivo* with [F-18]FLT and positron emission tomography. *Nat Med.* 1998;4:1334–1336.
9. Toyohara J, Kumata K, Fukushi K, Irie T, Suzuki K. Evaluation of [methyl-^{14}C]4′-thiothymidine for *in vivo* DNA synthesis imaging. *J Nucl Med.* 2006;47:1717–1722.
10. Toyohara J, Okada M, Toramatsu C, Suzuki K, Irie T. Feasibility studies of 4′-[methyl-^{11}C]thiothymidine as a tumor proliferation imaging agent in mice. *Nucl Med Biol.* 2008;35:67–74.
11. Toyohara J, Nariai T, Sakata M, et al. Whole-body distribution and brain tumor imaging with ^{11}C-4DST: a pilot study. *J Nucl Med.* 2011;52:1322–1328.
12. Vesselle H, Grierson J, Peterson LM, Muzi M, Mankoff DA, Krohn KA. ^{18}F-fluorothymidine radiation dosimetry in human PET imaging studies. *J Nucl Med.* 2003;44:1482–1488.
13. Costa A, Silvestrini R, Mochen C, et al. P53 expression, DNA ploidy and S-phase cell fraction in operable locally advanced non-small-cell lung cancer. *Br J Cancer.* 1996;73:914–919.
14. Weidner N, Semple JP, Welch WR, Folkman J. Tumor angiogenesis and metastasis: correlation in invasive breast carcinoma. *N Engl J Med.* 1991;324:1–8.
15. Dosaka-Akita H, Hommura F, Mishina T, et al. A risk-stratification model of non-small cell lung cancers using cyclin E, Ki-67, and ras p21: different roles of G1 cyclins in cell proliferation and prognosis. *Cancer Res.* 2001;61:2500–2504.
16. Koole LH, Plavec J, Liu H, et al. Conformation of two 4′-thio-2′-deoxynucleoside analogs studied by 500-MHz ^{1}H NMR spectroscopy and x-ray crystallography. *J Am Chem Soc.* 1992;114:9936–9943.
17. Parker WB, Shaddix SC, Rose LM, et al. Metabolism and metabolic actions of 4′-thiothymidine in L1210 cells. *Biochem Pharmacol.* 1995;50:687–695.
18. Mier W, Haberkorn U, Eisenhut M. [^{18}F]FLT; portrait of a proliferation marker. *Eur J Nucl Med Mol Imaging.* 2002;29:165–169.
19. Rasey JS, Grierson JR, Wiens LW, Kolb PD, Schwartz JL. Validation of FLT uptake as a measure of thymidine kinase-1 activity in A549 carcinoma cells. *J Nucl Med.* 2002;43:1210–1217.

20. Buck AK, Halter G, Schirrmeister H, et al. Imaging proliferation in lung tumors with PET: ^{18}F-FLT versus ^{18}F-FDG. *J Nucl Med.* 2003;44:1426–1431.
21. Vesselle H, Schmidt RA, Pugsley JM, et al. Lung cancer proliferation correlates with [F-18] fluorodeoxyglucose uptake by positron emission tomography. *Clin Cancer Res.* 2000;6:3837–3844.
22. Higashi K, Ueda Y, Yagishita M, et al. FDG PET measurement of the proliferative potential of non-small cell lung cancer. *J Nucl Med.* 2000;41:85–92.
23. Yamamoto Y, Nishiyama Y, Ishikawa S, et al. Correlation of ^{18}F-FLT and ^{18}F-FDG uptake on PET with Ki-67 immunohistochemistry in non-small cell lung cancer. *Eur J Nucl Med Mol Imaging.* 2007;34:1610–1616.
24. Guo J, Higashi K, Ueda Y, et al. Microvessel density: correlation with ^{18}F-FDG uptake and prognostic impact in lung adenocarcinomas. *J Nucl Med.* 2006;47: 419–425. 25.
25. Goerres GW, Burger C, Kamel E, et al. Respiration-induced attenuation artifact at PET/CT: technical considerations. *Radiology.* 2003;226:906–910.
26. Nehmeh SA, Erdi YE, Ling CC, et al. Effect of respiratory gating on quantifying PET images of lung cancer. *J Nucl Med.* 2002;43:876–881.
27. Gilman MD, Fischman AJ, Krishnasetty V, Halpern EF, Aquino SL. Optimal CT breathing protocol for combined thoracic PET/CT. *AJR.* 2006;187: 1357–1360.